Synthesis and Characterization of a New Degradable Poly(ester amide) Derived from 6-Amino-1-hexanol and Glutaric Acid

Montserrat Vera, Ahmed Almontassir, Alfonso Rodríguez-Galán, and Jordi Puiggalí*

Departament d'Enginyeria Quimica, ETS d'Enginyeria Industrial, Universitat Politècnica de Catalunya, Diagonal 647, Barcelona E-08028, Spain

Received May 2, 2003; Revised Manuscript Received September 26, 2003

ABSTRACT: An alternating poly(ester amide) constituted by 6-amino-1-hexanol and glutaric units has been synthesized by different ways involving solution or thermal polycondensation. Results of the synthesis are compared, and the occurrence of a thermal degradation through imide ring formation is demonstrated. Hydrolytic and enzymatic degradation of the new polymer has been evaluated by means of weight loss measures and changes in intrinsic viscosity or by analysis of NMR spectra. Thermal properties and crystallization kinetics have also been studied. Crystalline structure has been investigated by X-ray fiber diffraction and electron microscopy of lamellar single crystals. Results indicate that polymorphism exists involving packing modes similar to those found on aliphatic polyamides.

Introduction

Poly(ester amide)s constitute a group of polymers with degradable properties that can replace polyesters in certain applications. Polyesters are nowadays the most important family of degradable polymers, but in general their thermal and mechanical properties are not optimal. This feature can be improved with the introduction of amide groups in the main chain, since they can give rise to strong intermolecular hydrogen bond interactions.

Different procedures are available to synthesize aliphatic poly(ester amide)s, namely the reaction between diols, dicarboxylic acids, and amino acids which has been extensively studied by our group when α-amino acids are involved[1−10] or the recent commercialization of BAK 1095 by Bayer, which corresponds to a random poly(ester amide) derived from 1,4-butanediol, adipic acid, and caprolactame.[11,12] Another possibility to get poly(ester amide)s is the reaction of alcohol amines with dicarboxylic acids. The first kinds of these derivatives correspond to the polymerization under reduced pressure of 2-aminoethanol or 3-amino-1-propanol and succinic, adipic, or sebacic acids.[13−15] Polymers with the additional inclusion of diols and caprolactame were patented in 1959 by BASF.[16] Fibers of 5-amino-1-pentanol derivatives were produced by Kodak[17] in 1960 by polycondensation with diesters at high temperature and vacuum. Since then, different poly(ester amide)s derived from amino alcohols have been produced and different applications have been utilized: photographic emulsions,[18] magnetic tapes,[19] adhesives,[20−22] dielectric materials,[23] biomedicine,[24] interfacial agents,[25] and additives for the paper industry.[26]

The monomer 6-amino-1-hexanol has been widely used due to the aminolysis reaction with copolymers of methacrylic acid or butyl methacrylate and styrene that give rise to a functionalization and a variation of properties.[27−29] Cell adhesion has been considered[30,31] and also the improvement of the optical properties of contact lens constituted by poly(2-hydroxyethyl methacrylate)[32] not to mention the preparation of membranes with good transport properties.[33]

In this work, we study the isoregic poly(ester amide) derived from 6-amino-1-hexanol and glutaric acid (named as *i*-PEAG6) taking into account degradability, main properties, and basic structural data. The main goal concerns the evaluation of conditions where the imide ring formation is feasible in both synthesis and degradation. Thus, different studies on related poly(ester amide)s derived from succinic acid and amino alcohols were carried out in our department, demonstrating that the degradation proceeded quickly due to the rapid formation of succinimide rings in the isoregic polymers[34] (Scheme 1a), which is an interesting feature. On the contrary, adirectional poly(ester amide)s characterized by the sequence $-NH(CH_2)_nOCO(CH_2)_2COO(CH_2)_n$-$NHCO(CH_2)_2CO-$ degraded at a slower rate due to the impossibility of cyclization. The degradation of the isoregic polymer constituted by 5-amino-1-pentanol and glutaric acid has recently been evaluated and shows a very slow degradation rate.[34] Conformational preferences of the succinamide,[35] succinate,[36] and glutaramide[37] units (Scheme 1b) may explain the different ability to produce imide rings and consequently the breakage of the polymer chain. Note that a single gauche torsional angle exists in the succinic derivatives giving rise to a bending of the molecules, whereas a pair of gauche angles with opposite signs are present in the glutaric derivatives.

Although the structures of polyamides and polyesters have been extensively studied, the reported structural data on poly(ester amide) are scarce. The long repeat units and the complexity derived from the different packing preferences of ester and amide groups[3] are limiting points. The structural study of different kinds of poly(ester amide)s appears also an interesting insight.

Experimental Section

Synthesis of *i*-PEAG6. We have compared different procedures to prepare this poly(ester amide): solution polycondensation, by the active ester method or using EDC·HCl as a condensing agent, and bulk thermal polycondensation.

Synthesis of *i*-PEAG6 by the Active Ester Method. Scheme 2 shows the preparation of the indicated poly(ester

* Corresponding author. E-mail: Jordi.Puiggali@upc.es.

10.1021/ma0345652 CCC: $25.00
Published on Web 11/26/2003

Scheme 1

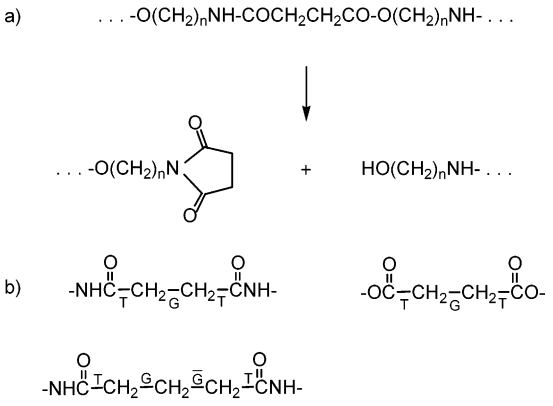

Scheme 2

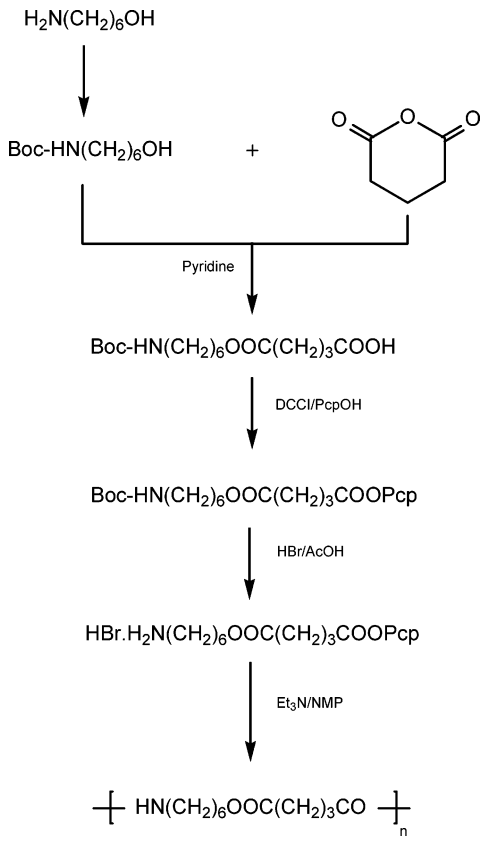

amide) by polycondensation in solution and following the active ester methodology. *tert*-Butoxycarbonyl (BOC) was selected as the amine protecting group, whereas pentachlorophenol was used to obtain the active ester.

N-tert-Butoxycarbonyl-6-aminohexanol (***I***). 60 mL of a dichloromethane solution of 0.11 mol of di-*tert*-butyl carbonate was dropwise added to the same volume of a solution of 0.1 mol of 6-amine-1-hexanol in dichloromethane. After 20 h of stirring at room temperature, the solution was diluted with 120 mL of diethyl ether and successively washed with a pH 5.4 sodium phosphate buffer (4 × 30 mL), a saturated water solution of Na_2CO_3 (1 × 60 mL), and a saturated water solution of NaCl (1 × 60 mL). The organic phase was dried with anhydrous Na_2SO_4 and evaporated under reduced pressure. A white solid was obtained with a yield of 66%.

IR (KBr, ν, cm^{-1}): 3347 (NH stretching), 2932 and 2861 (CH_2), 1688 (urethane C═O), 1526 (urethane NH), 1055 (C−O). ^{1}H NMR ($CDCl_3$, TMS, int ref): δ 4.56 (1H, NH), 3.63 (m, 2H, CH_2OH), 3.11 (m, 2H, CH_2NH), 1.55 (m, 2H, CH_2CH$_2$OH), 1.46 (m, 2H, CH_2CH$_2$NH), 1.44 (s, 9H, CH_3), 1.35 (m, 4H, CH_2-CH$_2$CH$_2$OH + CH_2CH$_2$ CH$_2$NH).

N-tert-Butoxycarbonyl-6-amino-1-hexyl Monoglutarate (***II***). A two-neck, round-bottom flask equipped with a magnetic stirrer, a $CaCl_2$ drying tube, and a condenser was charged with **I** (19.34 mmol), glutaric anhydride (19.34 mmol), 50 mL of chlorobenzene, and 7 drops of pyridine as catalyst.[38] The mixture was heated at 70 °C until complete dissolution of the glutaric anhydride and then prolonged the reaction for an additional 5 h. Evaporation to dryness of the organic solution yielded compound **II** as a colorless oil with a yield of 91%.

IR (KBr, ν, cm^{-1}): 3358 (NH stretching), 2935 and 2862 (CH_2), 1711 (acid C═O), 1688 (urethane C═O), 1526 (urethane NH), 1169 (C−O). ^{1}H NMR ($CDCl_3$, TMS, int ref): δ 4.62 (1H, NH), 4.15 (t, 2H, CH_2OCO), 3.13 (t, 2H, CH_2NH), 2.52 (m, 4H, CH_2COOH + CH_2COO), 2.00 (m, 2H, CH_2CH$_2$COO), 1.69 (m, 2H, CH_2CH$_2$OCO), 1.50 (s, 9H, CH_3), 1.40 (m, 2H, CH_2CH$_2$-NH), 1.36 (m, 4H, CH_2CH$_2$CH$_2$OCO + CH_2CH$_2$CH$_2$NH).

Pentachlorophenyl Ester of N-tert-Butoxycarbonyl-6-amino-1-hexyl Monoglutarate (***III***). To a solution of **II** (15 mmol) in ethyl acetate (45 mL) were added 15 mmol of pentachlorophenol and an ethyl acetate solution (25 mL) of dicyclohexylcarbodiimide (15 mmol). The mixture was left at room temperature under stirring until the total disappearance of the starting products in the thin-layer chromatographs (5 days). The precipitated dicyclohexylurea (DCU) was filtrated and the liquid concentrated to half volume. The additional DCU that precipitated was separated again, and the filtrate was successively washed with a saturated water solution of $NaHCO_3$ (2 × 10 mL) and distilled water (2 × 10 mL). The organic phase was dried with anhydrous Na_2SO_4, filtrated, and evaporated. The resulting solid was washed with ethyl ether and obtained with a yield of 79%; mp 63 °C.

IR (KBr, ν, cm^{-1}): 3375 (NH stretching), 2929 and 2855 (CH_2), 1737 (ester C═O), 1678 (urethane C═O), 1518 (urethane NH), 1093 (C−O). ^{1}H NMR ($CDCl_3$, TMS, int ref): δ 4.55 (1H, NH), 4.13 (t, 2H, CH_2OCO), 3.14 (m, 2H, CH_2NH), 2.81 (t, 2H, CH_2COOPcp), 2.52 (t, 2H, CH_2COOCH$_2$), 2.16 (m, 2H, CH_2CH$_2$COO), 1.68 (m, 2H, CH_2CH$_2$OCO), 1.53 (m, 2H, CH_2CH$_2$NH), 1.47 (s, 9H, CH_3), 1.39 (m, 4H, CH_2CH$_2$CH$_2$OCO + CH_2CH$_2$CH$_2$NH).

Pentachlorophenyl Ester of N-tert-Butoxycarbonyl-6-amino-1-hexyl Glutarate Hydrobromide (***IV***). 8 mmol of **III** was dissolved in 60 mL of glacial acetic acid containing 11% HBr. After 90 min of stirring at room temperature the solvent was removed under reduced pressure. The solid was washed with ethyl acetate and recrystallized from 2-propanol. Yield 78%; mp 126 °C.

IR (KBr, ν, cm^{-1}): 3430 (NH_3^+), 2947 (CH_2), 1726 (ester C═O), 1111 (C−O). ^{1}H NMR ($CDCl_3$, TMS, int ref): δ 6.85 (3H, NH_3^+), 4.23 (t, 2H, CH_2OCO), 3.22 (m, 2H, CH_2NH$_3^+$), 2.85 (t, 2H, CH_2COOPcp), 2.64 (t, 2H, CH_2COOCH$_2$), 2.19 (m, 2H, CH_2-CH$_2$COO), 1.82 (m, 2H, CH_2CH$_2$OCO), 1.75 (m, 2H, CH_2CH$_2$-NH), 1.48 (m, 4H, CH_2CH$_2$CH$_2$OCO + CH_2CH$_2$CH$_2$NH$_3^+$).

Solution Polycondensation of the Active Ester. 5 mmol of compound **IV** was dissolved in 1.9 mL of *N*-methylpyrrolidone, and an excess (2.5 × 5 mmol) of triethylamine was dropwise added. The stiff mixture was left at 37 °C for 10 days, stirring it occasionally with a glass rod. The polymer was recovered by precipitation with 2-propanol of a chloroform/formic acid solution (4/1 v/v) and repeatedly washed with chloroform, ethanol, water, methanol, and ethyl ether. Yield: 83%.

Synthesis of *i*-PEAG6 by Solution Polycondensation with EDC·HCl. Scheme 3 shows the preparation of the indicated poly(ester amide) by solution polycondensation and using *N*-ethyl-*N*-(3,3-(dimethylamino)propyl)carbodiimide hydrochloride (EDC·HCl) as activating reagent. This was selected due to fact that the generated urea subproduct could be easily separated by solubilization.

4-(6-Hydroxyhexylcarbamoyl)butyric Acid (***V***). To a solution of 0.02 mol of 6-amine-1-hexanol in 20 mL of chloroform was slowly added 20 mL of a solution of glutaric anhydride (0.02 mol) in the same solvent. The mixture was left to react under stirring for 3 days at room temperature. A white solid precipitated, which was isolated by filtration and recrystallized from ethyl acetate. Yield 64%; mp 89 °C.

Scheme 3

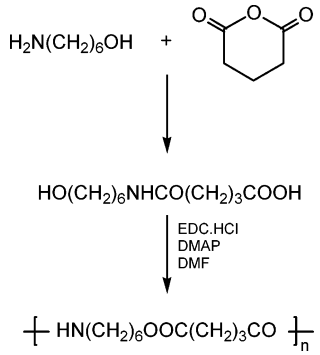

Scheme 4

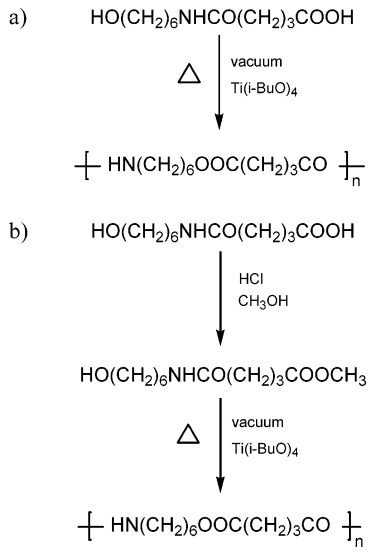

IR (KBr, ν, cm^{-1}): 3312 (amide A), 3053 (amide B), 2932 and 2858 (CH_2), 1696 (C═O), 1636 (amide I), 1536 (amide II), 1060 (C−O). ^{1}H NMR (TFA/$CDCl_3$, TMS, int ref): δ 7.90 (m, 1H, NH), 4.45 and 3.88 (2t, 2H, CH_2OH), 3.49 (m, 2H, CH_2-NH), 2.72 (t, 2H, CH_2CONH), 2.64 (t, 2H, CH_2COOH), 2.11 (m, 2H, CH_2CH$_2$COO), 1.83 (m, CH_2CH$_2$OH), 1.70 (m, CH_2-CH$_2$OH + CH_2CH$_2$NH), 1.45 (m, 4H, CH_2CH$_2$CH$_2$OH + CH_2-CH$_2$CH$_2$NH).

Solution Polycondensation of 4-(6-Hydroxyhexylcarbamoyl)-butyric Acid. A solution of **V** (4.4. mmol) and EDC·HCl (5.2 mmol) in dimethylformamide (2.2 mL) was stirred at 0 °C for 2 h. After that, 0.4 mmol of the catalyst 4-(dimethylamino)-pyridine (DMAP) was added to the solution and followed by stirring at room temperature for 8 h. The resulting mixture was poured into 0.1 M HCl aqueous solution (100 mL) to precipitate the polymer, which was separated by centrifugation and repeteadly washed with water, ethanol, and ethyl acetate. Yield: 80%.

Synthesis of *i*-PEAG6 by Thermal Bulk Polycondensation. Thermal polycondensation of both 4-(6-hydroxyhexylcarbamoyl)butyric acid and 4-(6-hydroxyhexylcarbamoyl)butyric acid methyl ester was investigated (Scheme 4).

4-(6-Hydroxyhexylcarbamoyl)butyric Acid Methyl Ester (***VI***). HCl was bubbled for 4 h into an anhydrous methanol solution (30 mL) of **V** (12 mmol). After that, the solution was stirred overnight and the solvent evaporated under reduced pressure. A pale yellow oil was obtained with a 90% yield.

IR (KBr, ν, cm^{-1}): 3270 (amide A), 3084 (amide B), 2936 and 2860 (CH_2), 1737 (C═O), 1644 (amide I), 1557 (amide II), 1055 (C−O). ^{1}H NMR (TFA/$CDCl_3$, TMS, int ref): δ 9.04 (1H, NH), 3.84 (t, 2H, CH_2OH), 3.62 (s, 3H, CH_3), 3.52 (m, 2H, CH_2-NH), 2.86 (t, 2H, CH_2CONH), 2.66 (t, 2H, CH_2COOCH$_3$), 2.08 (m, 2H, CH_2CH$_2$COO), 1.69 (m, 4H, CH_2CH$_2$OH + CH_2CH$_2$-NH), 1.42 (m, 4H, CH_2CH$_2$CH$_2$OH + CH_2CH$_2$CH$_2$NH).

Scheme 5

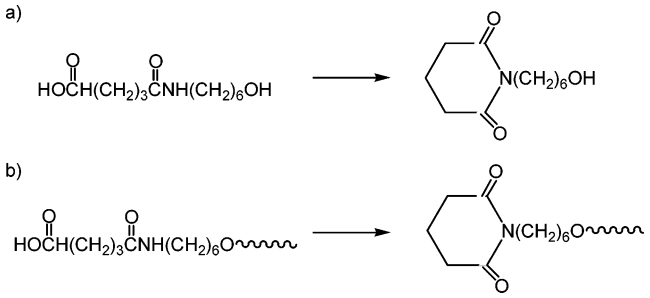

Thermal Bulk Polymerization. A two-neck, round-bottom flask equipped with a magnetic stirrer was charged with 2 mmol of compound **V** or **VI**. Titanium butoxide (0.3 mol %) was also added as a catalyst for the condensation reaction. The flask was heated in an oil bath at 150 °C in order to melt the mixture and to begin the esterification reaction. Meanwhile, a slow stream of nitrogen was passed to help eliminate water or methanol. After 2 h, the second neck was connected to a vacuum pump (0.3 mmHg). Different temperatures and reaction times were essayed. After cooling, the polymer was dissolved in formic acid, precipitated by a dropwise addition of ether, filtered, and repeatedly washed with ethanol, water, acetone, and ethyl ether.

Characterization. Intrinsic viscosities were determined with a Cannon-Ubbelohde microviscometer in dichloroacetic solutions at 25 ± 0.1 °C.

The molecular weight distributions (M_n, M_w, and polydispersity index) were measured with a GPC apparatus (Water Assoc., model 510 pump) equipped with a Millenium computer program. Average molecular weights are indicative because they were calculated using poly(methyl methacrylate) standards. A Styragel linear column (Water HR5E) and a RI 410 (Water Assoc.) detector were used. The polymers were dissolved and eluted in hexafluoro-2-propanol at a flow rate of 0.8 mL/min (injected volume 100 μL, sample concentration 0.10% w/v).

Infrared absorption spectra were recorded with a Perkin-Elmer 1600 FT-IR spectrometer in the 4000−500 cm^{-1} range from KBr disks or films prepared from evaporation of formic acid solutions. NMR spectra of polymers were registered from deuterated chloroform/trifluoroacetic acid solutions. Chemical displacements were calibrated using tetramethylsilane as an internal standard. A Bruker AMX-300 spectrometer operating at 300.1 and 75.5 MHz was used for ^{1}H and ^{13}C NMR investigations, respectively.

Thermal analysis was performed by differential scanning calorimetry with a Perkin-Elmer DSC-PYRIS 1, using indium metal for calibration. Heating and cooling runs were performed, except when it is explicitly indicated, under a flow of dry nitrogen at 20 and 10 °C/min, respectively. All crystallization rate studies were carried out on completely amorphous samples. Hot- and cold-crystallization studies refer to the isothermal crystallizations performed when samples were cooled (50 °C/min) from the melt state or heated (200 °C/min) from the glass state, respectively. In the last case, samples were previously quenched in liquid nitrogen from the melt.

Thermogravimetric analysis was carried out with a Perkin-Elmer TGA-6 thermobalance.

Fiber X-ray diffraction patterns were recorded in a vacuum at room temperature. Calcite (d_B = 3.035 Å) was used for calibration. A modified Statton camera (W.H. Warhus, Wilmington, DE) with nickel-filtered radiation of 1.542 Å was used for these experiments.

Isothermal crystallizations were carried out in the 30−70 °C range from dilute solutions (0.01% w/v) in 1,4-butanediol. The crystals were recovered from the mother liqueur by centrifugation, repeatedly washed with 1-butanol, and deposited on carbon-coated grids, which were shadowed with Pt−carbon at an angle of 15° for bright field observations.

Solution-grown spherulites were obtained by slow evaporation from a drop of formic acid solution (5%, w/v) placed

Table 1. Reaction Conditions, Yields, and Intrinsic Viscosities of *i*-PEAG6

method	temp (°C)	time (h)	yield (%)	[η] (dL/g)
solution polycondensation using PcpOH as the active ester	37	240	83	1.06
solution polycondensation using EDC·HCl as a coupling agent	25	8[a]	85	0.31
thermal polycondensation of compound **V**	150	20[b]	65	0.43
thermal polycondensation of compound **V**	180	10[b]	50	0.27
thermal polycondensation of compound **V**	180	20[b]	70	0.50
thermal polycondensation of compound **V**	180	30[b]	53	0.44
thermal polycondensation of compound **V**	200	20[b]	55	0.30
thermal polycondensation of compound **VI**	180	20[b]	60	0.39
thermal polycondensation of compound **VI**	200	20[b]	50	0.24

[a] Polymerization was previously carried out for 2 h at 0 °C. [b] Polymerization was previously carried out for 2 h at 150 °C under a nitrogen stream before the indicated time and temperature, which were applied under vacuum.

between the coverslip and the slide. Spherulites were also grown from melt-crystallized films produced by heating 5 mg of polymer on microscope slides. When the polymer was molten, the films were pressed or smeared between coverslips and slides. The films were crystallized isothermally at different temperatures below the melting point using a Mettler FP80 thermal analysis instrument. This procedure allows us to obtain films with a regular thickness close to 40 μm. Optical photographs were taken using an Olympus BX5 light polarizing microscope equipped with an Olympus C3030Z digital camera. A first-order red tint plate was used to determine the sign of spherulite birefringence under crossed polarizers.

A Philips TECNAI 10 electron microscope was used and operated at 80 and 100 kV for bright field and electron diffraction modes, respectively. Selected area electron diffraction patterns were recorded on Kodak Tri-X films. The patterns were internally calibrated with gold (d_{111} = 0.235 nm).

Samples for hydrolytic and enzymatic degradation studies were cut off from regular films of 200 and 70 μm of thickness, respectively, prepared by melt pressing 200 or 70 mg of the polymer at a temperature of 10 °C below fusion. Plate samples of 15 mm × 15 mm were usually employed in the degradation experiments.

Hydrolytic degradation assays were carried out under the accelerated conditions provided by distilled water at 70 °C. Each plate was kept in a bottle filled with 30 mL of the aqueous media and sodium azyde (0.03 wt %) to prevent microbial growth. After the immersion time, the retrieved samples were thoroughly rinsed with distilled water, dried to constant weight in a vacuum, and stored over $CaCl_2$ before analysis.

Enzymatic degradation studies were conducted at 37 °C by using a lipase from *Pseudomonas cepacia* (LPC) or a proteolytic enzymes such as proteinase K. The enzymatic media, 10 mL, consisted of a sodium phosphate buffer (pH 7.2) containing sodium azide (0.03 wt %) and 1 mg of the appropriate enzyme. All enzymatic solutions were renewed every 72 h because of enzymatic activity loss. After the immersion time, the retrieved samples were immersed in a HCl solution (pH, 2), rinsed with water, and dried as indicated for hydrolytic experiments.

Mass loss, intrinsic viscosity, and changes in the NMR spectra were evaluated in these degradation studies. Scanning electron microscopy was employed to examine the changes in the texture of samples after degradation. Gold coating was accomplished by using a Balzers SCD-004 sputter coater. The SEM micrographs were carried out with a JEOL JSM-6400 instrument.

Results and Discussion

Synthesis. Polymers obtained by the ester active method had a good polymerization yield and also the highest intrinsic viscosity, as shown in Table 1. A value of 1.06 dL/g, measured in dichloroacetic acid at 25 °C, could be attained under the indicated experimental conditions. The GPC analysis gives number- and weight-average molecular weights of 15 100 and 32 900 g/mol, respectively, which correspond to a polydispersity of 2.2. The material had good fiber- and film-forming properties, in agreement with its high molecular weight, and was selected for latter studies that involve thermal properties, degradation studies, crystallization kinetics, and structural data. Basic solubility data are summarized in Table 2.

Table 2. Basic Solubility Data of *i*-PEAG6

solvent[a]	insoluble	swell up	soluble at HT[b]	soluble at RT[b]
water	+			
ethyl ether	+			
ethyl acetate	+			
acetone	+			
chloroform		+		
dichloromethane		+		
ethanol			+	
DMF			+	
DMSO			+	
NMP			+	
formic acid				+
DCA				+
TFA				+
TFE				+
HFIP				+

[a] DMF = dimethylformamide; DMSO = dimethyl sulfoxide; NMP = *N*-methylpyrrolidone; DCA = dichloroacetic acid; TFA = trifluoroacetic acid; TFE = trifluoroethanol; HFIP = hexafluoro-2-propanol. [b] HT = high temperature; RT = room temperature.

Infrared and ^{1}H NMR spectra fully agree with the anticipated chemical constitution:

IR (KBr, ν, cm^{-1}): 3312 (amide A), 3086 (amide B), 2936 and 2864 (CH_2), 1732 (C═O), 1640 (amide I), 1548 (amide II), 1183 (C−O). ^{1}H NMR (TFA/$CDCl_3$, TMS, int ref): δ 8.81 (1H, NH), 4.36 (2H, CH_2OCO), 3.65 (2H, CH_2NH), 2.90 (2H, CH_2CONH), 2.75 (2H, CH_2COO), 2.21 (2H, CH_2CH$_2$COO), 1.82 (4H, CH_2CH$_2$O + CH_2-CH$_2$NH), 1.55 (4H, CH_2CH$_2$CH$_2$O + CH_2CH$_2$CH$_2$NH). ^{13}C NMR (TFA/$CDCl_3$, TMS, int ref): δ 178.11 (CONH), 177.84 (COO), 67.07 (CH_2O), 42.53 (CH_2NH), 32.70 + 32.49 (*C*H$_2$CONH + *C*H$_2$COO).

Furthermore, no signals attributed to terminal groups could be detected in both ^{1}H and ^{13}C NMR spectra (Figure 1a,b).

A lower molecular weight was attained in the solution polymerization carried out by using EDC.HCl as a condensing agent. Thus, intrinsic viscosity decreases to 0.31 dL/g and molecular weights to 10 140 and 4430 g/mol for M_w and M_n, respectively. In the same way, terminal groups associated with both hydroxyl and carboxyl terminal groups were detected in the ^{1}H NMR spectra, allowing to infer a number-average molecular weight of 3500 g/mol.

The thermal stability of 4-(6-hydroxyhexylcarbamoyl)-butyric acid was studied by static thermogravimetry under a N_2 flow. The results indicate that the monomer was stable at temperatures close to 150 °C, since no

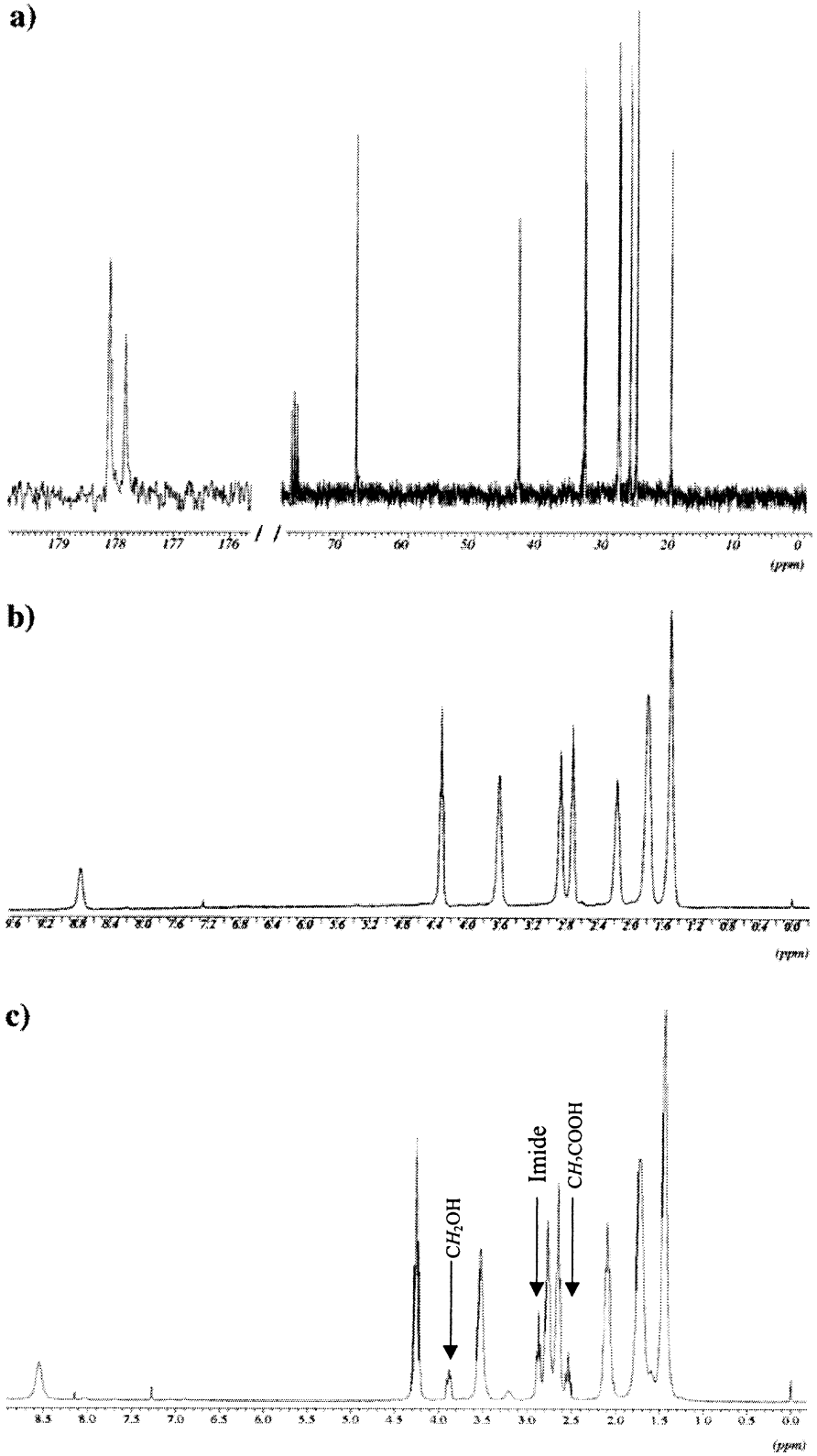

Figure 1. ^{13}C NMR (a) and ^{1}H NMR (b) spectra of *i*-PEAG6 obtained by the active ester method. (c) ^{1}H NMR spectra of a polymer, intrinsic viscosity of 0.24 dL/g, prepared by thermal polyesterification of compound **VI**. Arrows indicate signals corresponding to cyclic imide rings and $-CH_2OH$ and $-CH_2COOH$ terminal groups. Polymer signals appear slightly shifted due to their variability with the solvent composition.

weight loss was detected after 3 h of thermal treatment, and no imide peaks or other anomalous signals could be observed in the corresponding ^{1}H NMR spectra.

Thus, thermal polymerizations were assayed for different times and temperatures close to 150 °C or higher, but under vacuum to favor the condensation reactions. The results summarized in Table 1 show that the highest intrinsic viscosity could be attained at 180 °C for 20 h of polymerization. In general, reaction does not progress when the time is short or the temperature is low, whereas some degradation occurs at high temperatures and long reaction times, since the medium takes

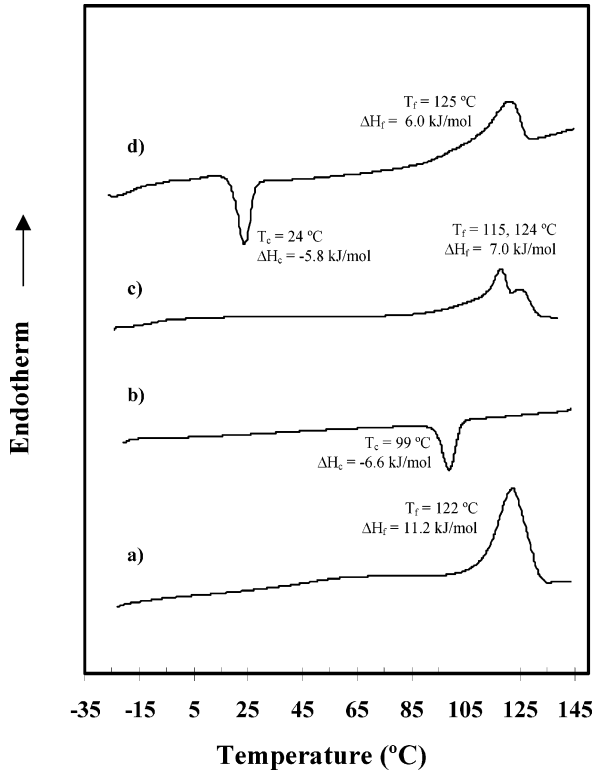

Figure 2. Sequence of four DSC scans performed with a *i*-PEAG6 sample obtained by the ester active method: (a) first heating run, (b) cooling run, (c) second heating run, (d) third heating run.

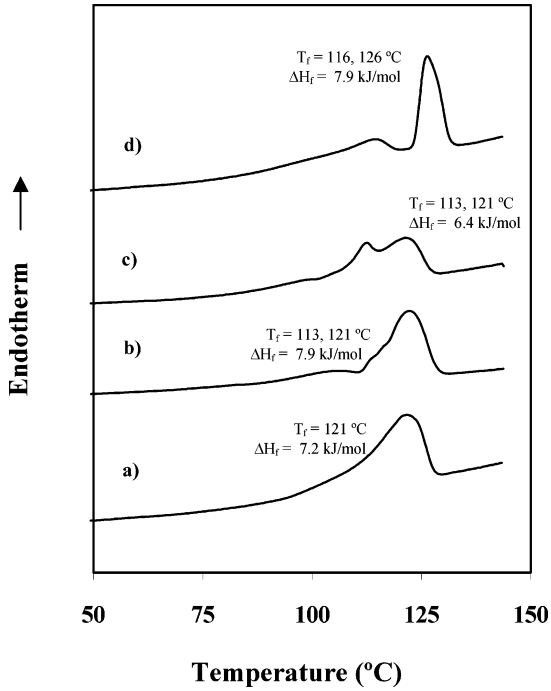

Figure 3. DSC heating runs of *i*-PEAG6 samples obtained by the ester active method after (a) isothermal crystallization at 9 °C, (b) isothermal crystallization at 109 °C, (c) isothermal crystallization at 101 °C, and (d) annealing at 120 °C for 15 min of a sample nonisothermally crystallized (cooling rate of 10 °C/min) from the melt state.

progressively a brown coloration. Furthermore, a waxy white product condenses in the flask wall at polymerization temperatures near 180 °C. This was identified by NMR spectroscopy (TFA/$CDCl_3$) as the *N*-(6-hydroxyhexyl)imide compound produced by monomer cyclization (Schema 5a); the imide ring signals appeared at 2.87 ppm for CH_2CO and 2.07 ppm for CH_2CH_2CO. In the same way, the glutaric end groups of a growing polymer chain could partially be cyclizated (Schema 5b), giving imide terminal groups that modifies the COOH/OH ratio and restricts the final molecular weight.

Imide ring formation is clearly enhanced in the thermal polymerization of 4-(6-hydroxyhexylcarbamoyl)-butyric acid methyl ester, and consequently lower molecular weights are attained, as shown in Table 1. ^{1}H NMR spectra clearly show the appearance of the CH_2CO imide signal at 2.87 ppm (Figure 1c) together with the CH_2OH end group at 3.88 ppm. Analysis of the appropriate signal areas for the sample with an intrinsic viscosity of 0.24 dL/g indicates an average molecular weight of 2200 g/mol ($(A_{4.26} + A_{3.88}) \times 213/A_{3.88}$)) and a cyclization of approximately 13% of the glutaric units ($A_{2.87} \times 100/(A_{2.87} + 2A_{2.77})$).

Thermal Properties. Thermal characterization of the new polymers was performed following a well-established protocol that involves four scans (Figure 2): first, a heating run of a sample as obtained from polymerization; second, a cooling run of the sample that was kept 2 min in the melt state; third, a new heating run to obtain data for the melt crystallized sample; and fourth, a heating run of a sample quenched in liquid nitrogen from the melt state. Data corresponding to the first scan are variable between polymers obtained from the different synthesis (solution- or melt-crystallized samples), whereas the results of the second and third heating runs are comparative due to the same thermal treatment after fusion. A melting temperature of 122 °C and a fusion enthalpy of 11.2 kJ/mol were determined for the solution-crystallized sample obtained by the active ester. The last value corresponds to a crystallinity close to 30% when the heat of fusion of a 100% crystalline material (35.5 kJ/mol) was estimated from the group contribution theory[39] (amide, 2 kJ/mol; methylene, 4 kJ/mol; ester −2.5 kJ/mol). The crystallinity decreases to approximately 20% when the sample is crystallized from the melt state, giving rise to two melting peaks at 118 and 126 °C. A supercooling close to 25 °C is required to crystallize the sample from the melt state (T_c = 99 °C), whereas crystallization takes place at 24 °C when it is performed by heating the melt quenched sample. In this case, a glass transition temperature of −18 °C is detected and again a unique melting peak at 125 °C, which the enthalpy indicates a crystallinity of 17%.

DSC traces were highly sensitive to thermal treatment (Figure 3), varying the ratio area between the two observed melting peaks. Thus, cold-crystallized samples show only the high-temperature peak, which also develops preferentially in hot crystallizations performed at temperatures higher than 107 °C. On the contrary, at higher undercoolings the low-temperature melting peak develops, as was also observed in the nonisothermal crystallization from the melt state (Figure 2c). However, when this sample was annealed at 120 °C (a temperature intermediate between the two fusion peaks), the ratio of the high melting peak increases. In all cases, the total heat of fusion remains practically constant, and thus only small variations in the degree of crystallinity were found (18−22%).

The observed multiple endotherms can be explained assuming a recrystallization process that affects the proportion between populations of crystals with a dif-

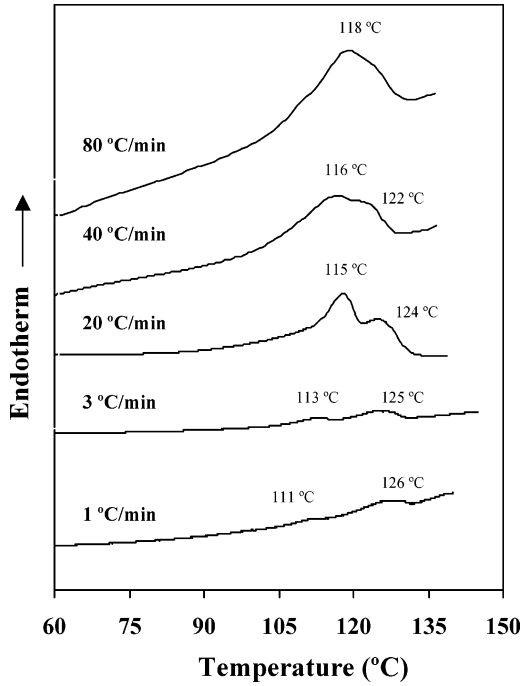

Figure 4. DSC runs, performed at the indicated heating rates, of *i*-PEAG6 samples previously crystallized from the melt state.

ferent lamellar thickness, as is usually observed in polyamides. DSC experiments performed at different heating rates with melt-crystallized samples (Figure 4) show that the low melting tempereature peak becomes more important, as the heating rate increases while the total enthalpy of fusion remains practically constant. This is the familiar pattern associated with reorganization during heating and indicates that at high rates the recrystallization toward the more stable state with thicker crystals (high melting temperature) is hindered. It can also be observed as both fusion peaks comes together with increasig the heating rate. In addition, the performed X-ray diffraction experiments were unsuccessful in order to associate the different peaks to polymorphism.

Thermal Stability. Dynamic thermogravimetric analysis of *i*-PEAG6 (Figure 5a) shows that decomposition begins at a temperature of 300 °C, whereas the half weight loss and the total decomposition are attained at 435 and 510 °C, respectively. These values are clearly higher than the melting temperature (more than 200 °C), and consequently the polymer is stable through fusion and can be processed from the melt state.

Figure 5b shows the static thermogravimetries carried out in a temperature range from 200 to 300 °C to see the effect of time on the thermal stability. It can be seen that no significant weight losses are detected after 2 h at 200 °C (3%) or 250 °C (5%). However, decomposition becomes important at 300 °C, since a 27.5% weight loss is reached after the same period of time. These results are in agreement with the reported dynamic analysis. Figure 5c shows also the ^{1}H NMR spectra of the thermally degraded sample, where it can be seen that peaks at 2.90 and 2.07 ppm, associated with glutarimide rings, and also signals at 3.91 and 3.63 ppm, indicative of ester and amide bond cleavages, appear.

Hydrolytic and Enzymatic Degradation Studies. Figure 6 shows the remaining weight percentages (a)

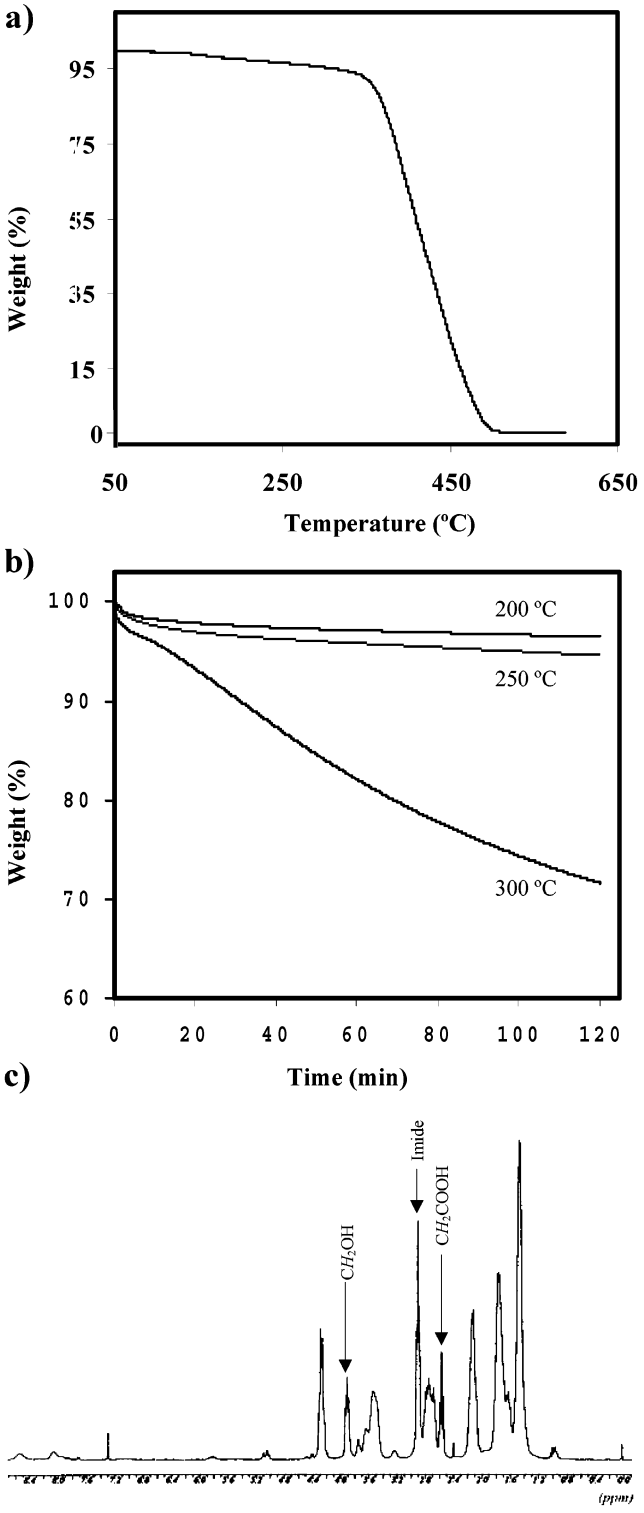

Figure 5. Dynamic (a) and static (b) thermogravimetric traces of *i*-PEAG6 synthesized by the active ester method. (c) ^{1}H NMR spectra of *i*-PEAG6 after keeping it at 300 °C for 2 h and under a nitrogen stream. Arrows indicate signals attributed to a cyclic imide and the terminal groups produced by cleavage of amide and ester bonds.

and the changes in intrinsic viscosity (b) of *i*-PEAG6 samples after immersion in distilled water at 70 °C. The results clearly demonstrated that this polymer degrades under the accelerated conditions provided by the high-temperature medium. Degradation products appear soluble, since a 50% weight loss was attained after 75 days of exposure. Intrinsic viscosity measures are highly

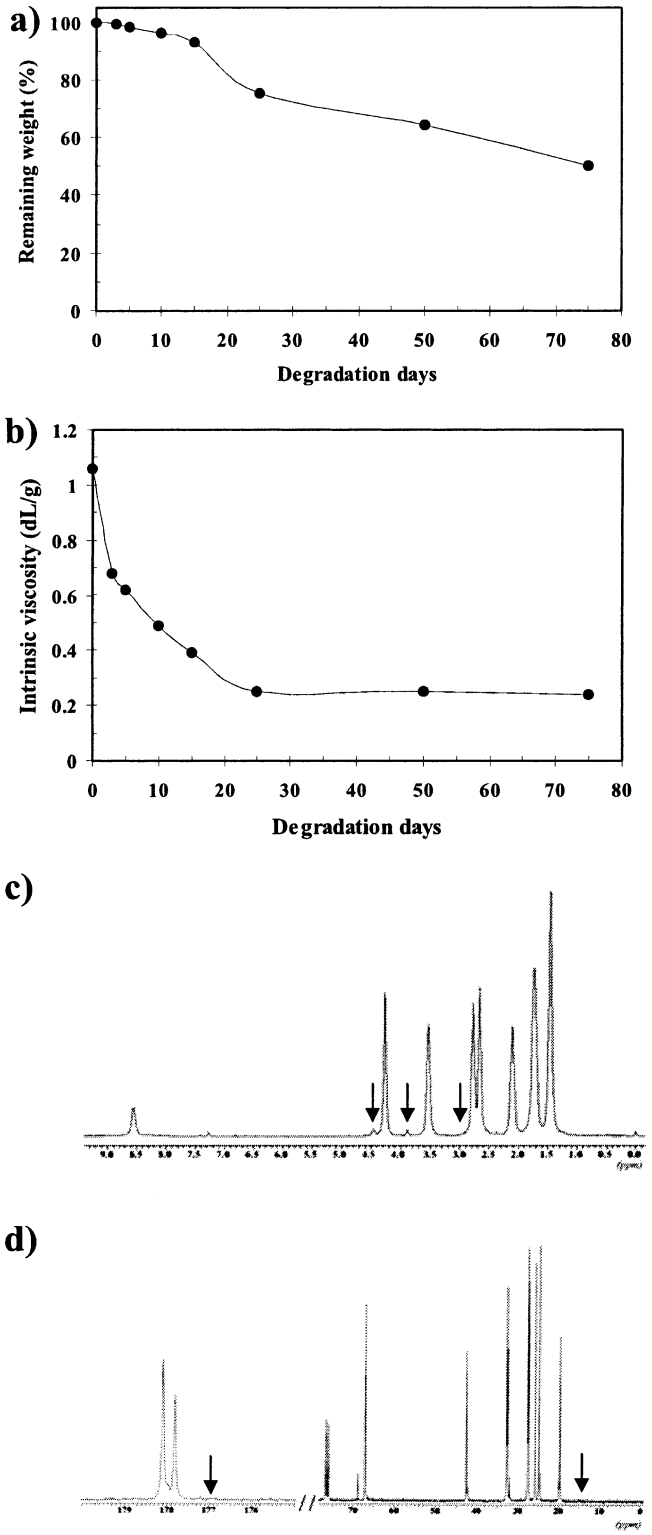

Figure 6. Remaining weight percentages (a) and intrinsic viscosity (b) of *i*-PEAG6 samples vs the days of exposure in distilled water at 70 °C. (c) ^{1}H NMR spectra of *i*-PEAG6 after 25 days of degradation in the indicated medium. (d) ^{13}C NMR spectra of *i*-PEAG6 after 25 days of degradation in the indicated medium. Arrows in (c) and (d) indicate main terminal groups and the expected signals for imide rings.

sensitive for evaluating degradation, since changes are clearly visible in the first stages. Thus, viscosity falls from 1.06 to 0.68 dL/g during the first 3 days of degradation. However, it must be indicated that the average molecular weight highly decreases with the

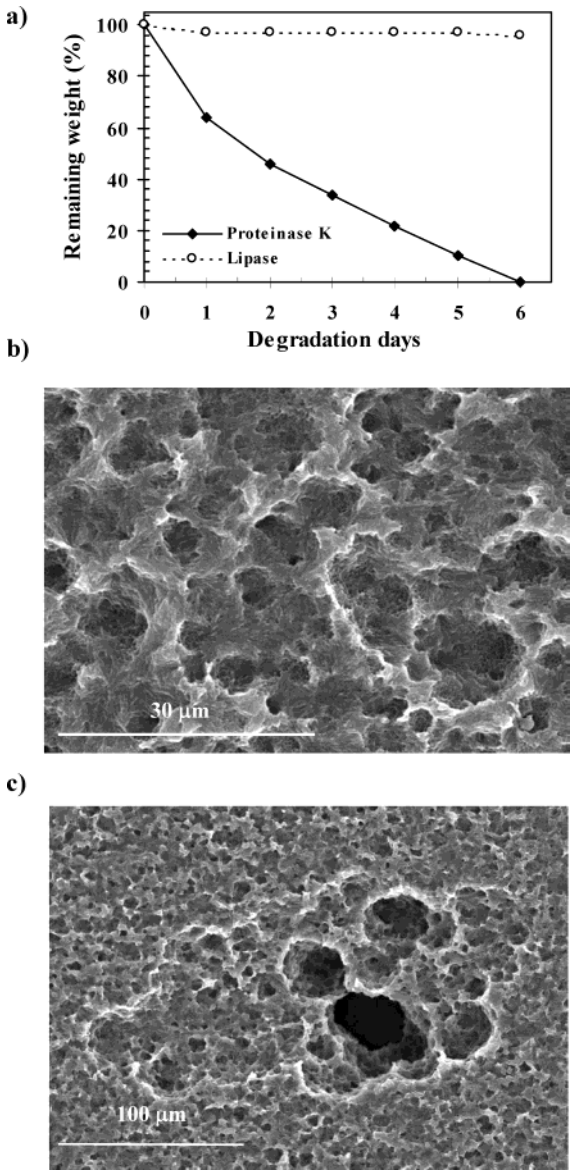

Figure 7. (a) Remaining weight percentages of *i*-PEAG6 exposed to lipase from *Pseudomona Cepacia* and proteinase K. (b, c) Scanning electron micrographs of *i*-PEAG6 exposed to proteinase K for 3 days.

cleavage of a reduced number of bonds for each molecular chain, and consequently viscosity is highly affected. Furthermore, the classical relationship between intrinsic viscosity and molecular weight ($[\eta] = KM_v^a$) indicates that the variation on the intrinsic viscosity will be more drastic when samples with high molecular weight are involved. Thus, viscosity decreases to only 0.39 dL/g during the next 12 days of degradation. Finally, a constant value close to 0.25 dL/g (25 days) is reached, indicating probably a limited molecular size for solubilization.

^{1}H NMR spectra show that degradation of *i*-PEAG6 takes place mainly through the cleavage of ester linkages. Thus, small signals can be detected at 4.48 and 3.88 ppm (Figure 6c), which correspond to the terminal CH_2OCOCF_3 and CH_2OH groups, respectively. No imide signals could be detected, an assessment that was verified from the ^{13}C NMR spectrum (Figure 6d). This shows the presence of CH_2OH (68.83 ppm) as the main terminal groups and no traces of imide ring signals (177.04 ppm for CO and 16.24 ppm for CH_2CON). It

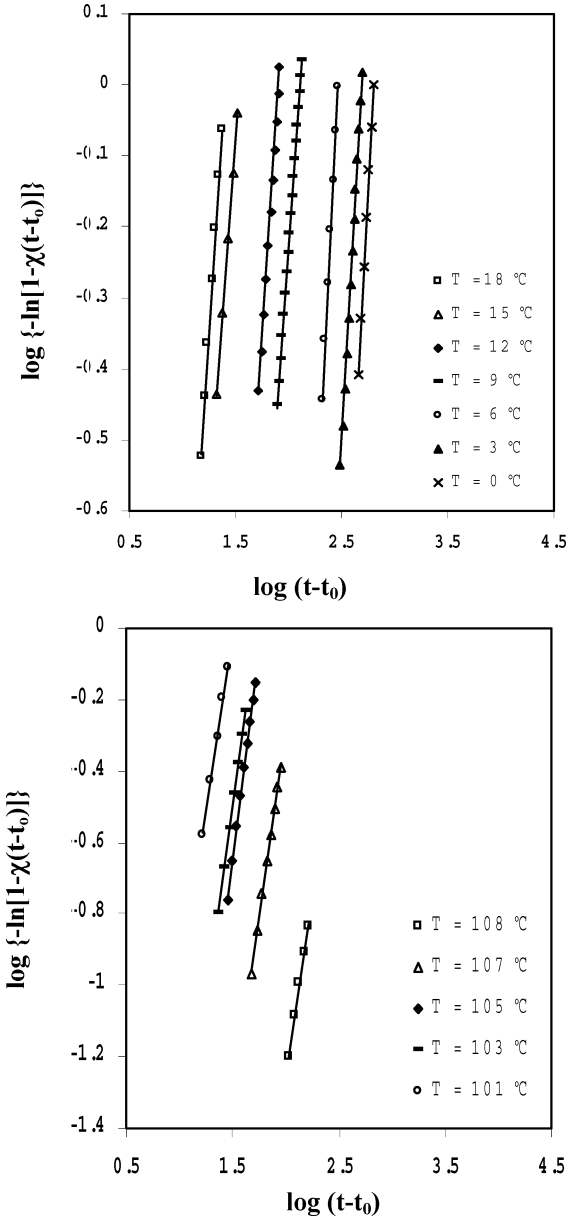

Figure 8. Avrami analysis for cold (up) and hot crystallization (down).

Table 3. Characteristic Data of DSC for Isothermal Crystallization of *i*-PEAG6

T (°C)	n	$Z \times 10^6$ (s^{-n})	$k \times 10^3$ (s^{-1})	$(t_{1/2}{}^a - t_0)$ (min)
0	2.79	0.015	1.75	9.30
3	2.77	0.035	2.03	7.20
6	2.82	0.104	3.34	4.30
9	2.11	35.54	7.78	1.80
12	2.34	34.42	12.37	1.15
15	2.02	778.39	28.91	0.49
18	2.35	521.67	40.10	
101	2.02	905.73	31.15	0.47
103	2.27	126.50	19.18	
105	2.27	90.42	16.54	1.04
107	2.11	31.06	7.30	2.10
108	1.88	9.94	2.18	7.25

[a] Time at which crystallinity reach 50%.

should be indicated that a mechanism involving an imide ring formation was deduced for related polymers derived from succinic acid,[34] which was responsible of an extremely quick degradation rate. The present study carried out under accelerated degradation conditions

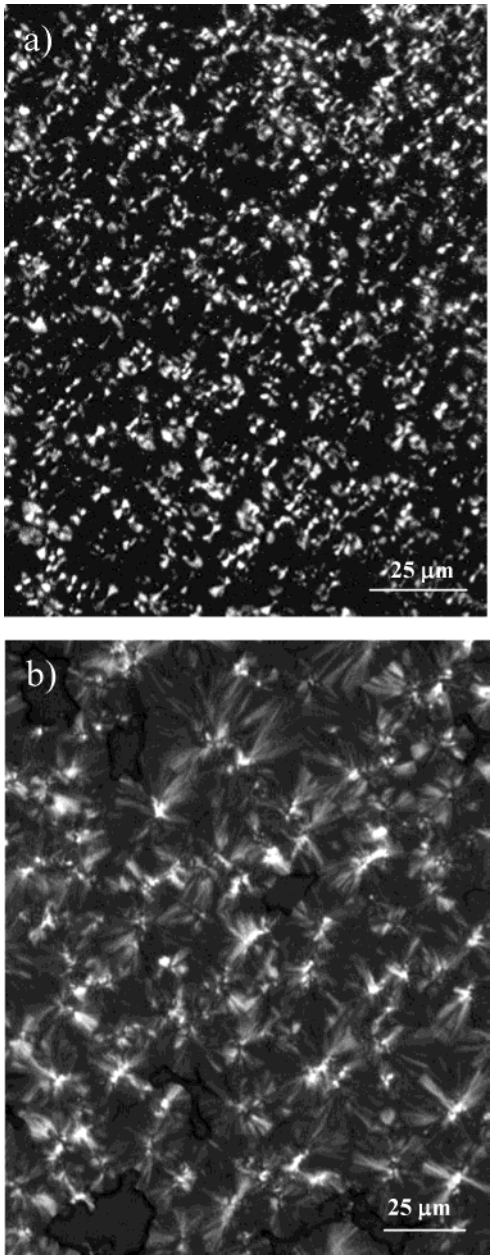

Figure 9. Optical micrographs of *i*-PEAG6 spherulites isothermally crystallized at 109 °C (a) and prepared by slow evaporation of a formic acid solution (b).

demonstrates that the mechanism cannot be extrapolated to the glutaric derivatives.

Degradation of *i*-PEAG6 was also studied in different media containing enzymes with an estearase (lipase from *Pseudomonas cepacia)* or a protease (proteinase K) activity. Degradation was only evaluated through the weight loss and the inspection of the scanning electron micrographs, since it is a surface process due to the large molecular size of enzymes. Figure 7a demonstrates that proteinase K is highly effective, since total solubilization of the *i*-PEAG6 samples is observed after 6 days of exposure. On the contrary, only a 4% weight loss was detected after exposition to lipase for the same period of time. Scanning electron micrographs (Figure 7b,c) also demonstrate the erosion and the surface attack of the proteinase K enzymatic medium. Thus, numerous hollows appear in the sample after 3 days of exposition that correspond to a solubilization of 64% of the material which is just the moment before the breakage of the

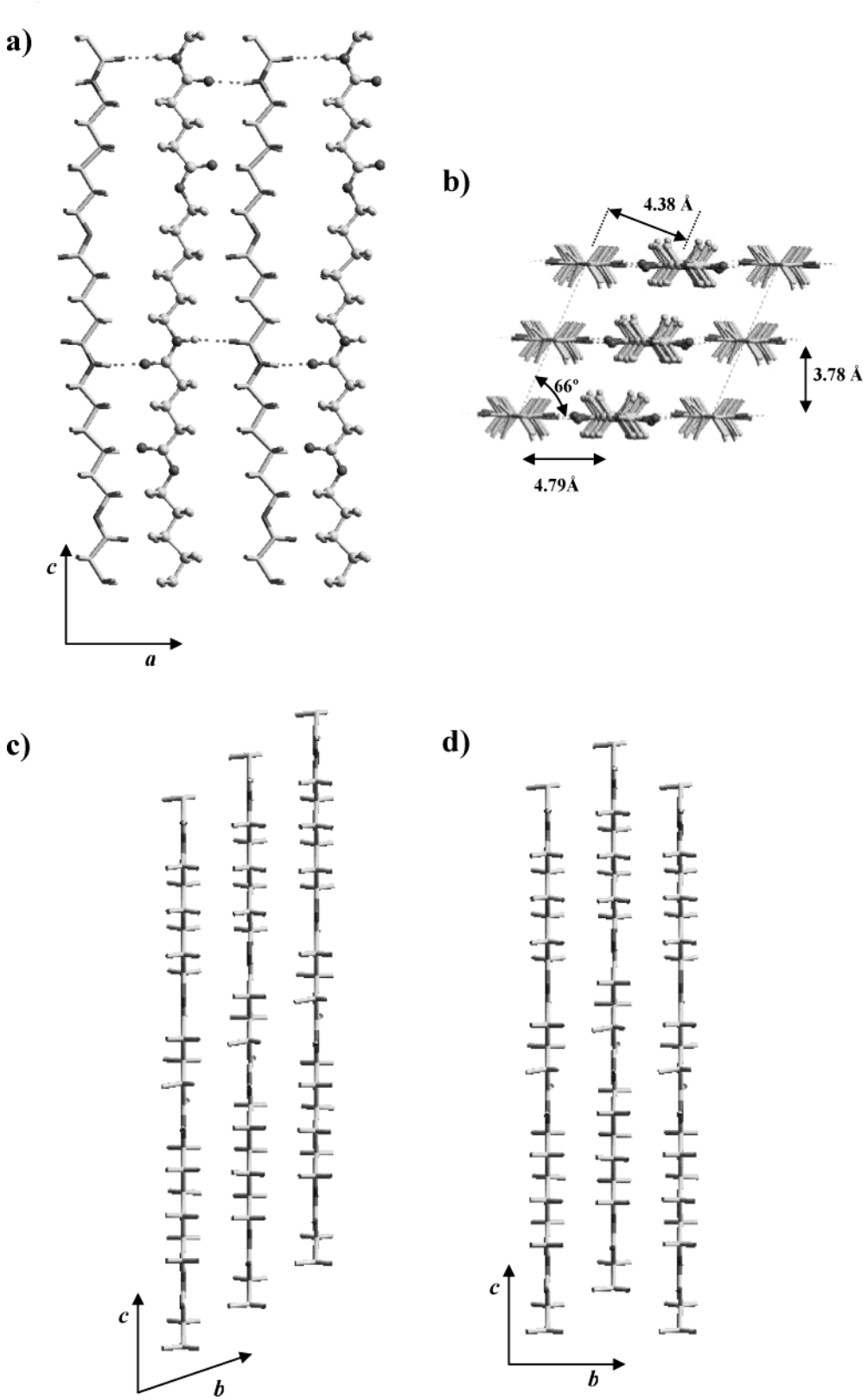

Figure 10. Schematic representation of the sheet arrangement between antiparallel molecular chains (a), the chain axis projection of the monoclinic unit cell (b), and the progressive (c) and the recuperative (d) sheet stackings of *i*-PEAG6. Main deduced spacings, angles, and distances are shown. Dashed lines indicate hydrogen bond interactions, whereas different representation styles are used for up and down molecular chains. Molecules have been drawn with an hypothetical all-trans conformation.

film. It can also be seen in Figure 7c the mechanism of the progressive erosion of the surface and the apparition of holes that cross all the film.

Isothermal Crystallization. The evolution of the weight fraction crystallinity vs time, $\chi(t - t_0)$, was calculated following the established methodology from cold- and hot-crystallization endotherms. Crystallization takes place at a very high rate between 18 and 101 °C, making unfeasible an accurate analysis in this temperature range.

Kinetic crystallization data were analyzed assuming the well-known Avrami equation[40] for the primary crystallization:

$$1 - \chi(t - t_0) = \exp[-Z(t - t_0)^n] \qquad (1)$$

where Z is the temperature-dependent rate constant, t_0 is the time when crystallization begins, and n is the Avrami exponent whose value varies according to crystallization mechanism. A normalized rate constant, $k = Z^{1/n}$, was also evaluated, since its dimension (time^{-1}) is independent of the value of the Avrami exponent.

The Avrami plots shown in Figure 8 give straight lines that allow to deduce the kinetic parameters summarized in Table 3. A maximum crystallization rate could be estimated at 50 °C, assuming a conventional bell-shaped curve to fit the dependence between the kinetic rate constant and the isothermal crystallization temperature.

Spherulites could be obtained when samples crystallize from the melt state, in agreement with the mean value of 2.3 for the Avrami exponent. A negative birefingence is observed, as usual for polyesters[41] and also for different poly(ester amides).[1,42] Numerous nuclei appear and spherulites quickly develop, reaching a small diameter (Figure 9a) that makes difficult an accurate analysis of the crystal growth. Solution-grown spherulites are also negative but can reach a larger diameter if the solvent evaporation is slow (Figure 9b).

Structural Data. X-ray and crystal electron diffraction patterns of *i*-PEAG6 demonstrate that crystal packings similar to those reported for the α and β structures of even nylons[43,44] are stabilized in both fiber and solution-crystallized samples. These structures are described by a stacking, with a progressive or a recuperative shift along the chain axis direction, of hydrogen-bonded sheets constituted by an antiparallel molecular chain arrangement (Figure 10).

Fiber X-ray diffraction patterns (Figure 11a,b) vary according to the treatment of the sample and agree with a monoclinic structure (recuperative stacking) with parameters $a = 9.58$ Å, $b = 8.28$ Å, c (chain axis) $= 30.3$ Å, $\alpha = 90°$, $\beta = 90°$, and $\gamma = 66°$ and a triclinic structure (progressive stacking) with parameters $a = 9.58$ Å, $b = 4.88$ Å, c (chain axis) $= 30.3$ Å, $\alpha = 58°$, $\beta = 90°$, and $\gamma = 70°$.

The chain axis repeat is the same for both structures (30.3 Å) and corresponds to two chemical repeat units. This periodicity is consistent with the value of 2.33 Å deduced from the intense 13th layer line, which is slightly shorter than the expected one for a fully extended conformation (2.46 Å). Thus, some torsion angles may deviate from 180°, giving rise to a slight rotation of amide and/or ester planes from that defined by the methylene carbons.

The two structures can be well distinguished taking into account the 002 reflections, since they appear with a meridional or a nonmeridional orientation for the monoclinic and triclinic forms, respectively. In the second case a *cc** angle of 32° can be measured, indicating a chain axis shift close to 2.60 Å (between two and three chemical bonds), as reported for different nylons and model compounds.[44,45]

The presence of 10*l* reflections is also remarkable, since their spacings are indicative of an antiparallel molecular chain arrangement. Fiber patterns are also characterized by the intense equatorial reflections at

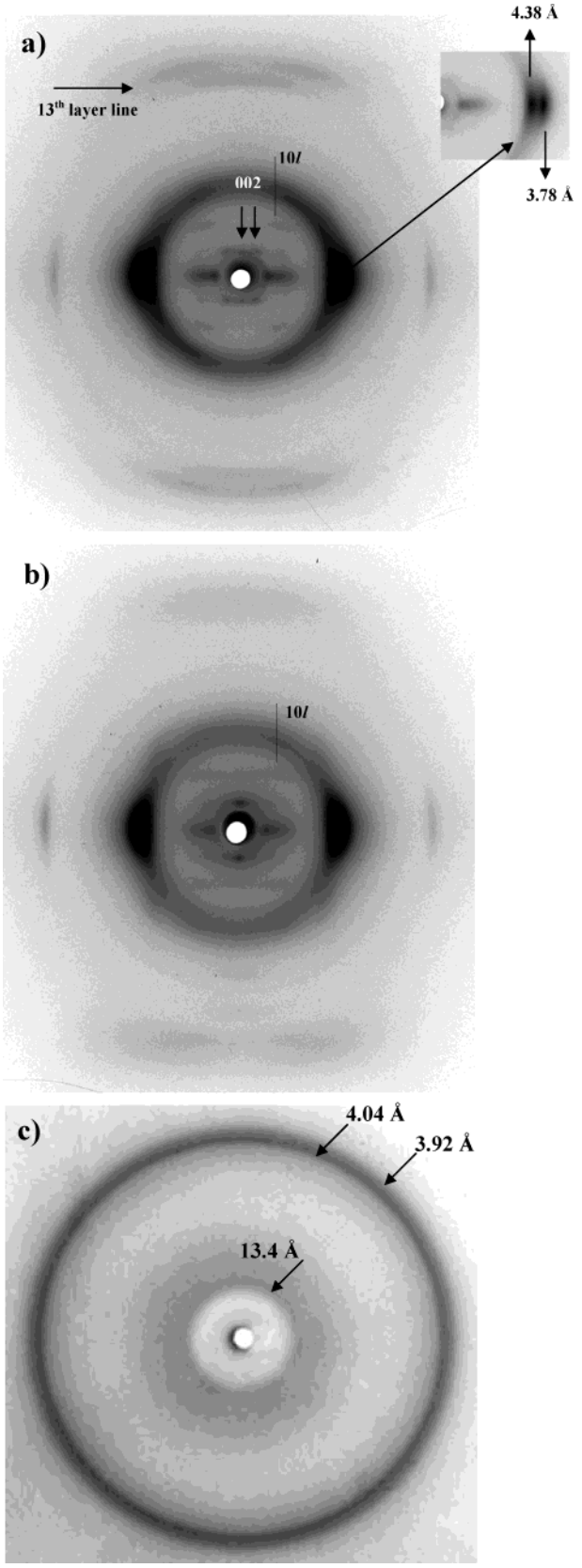

Figure 11. X-ray diffraction patterns of a melt-spun fiber (a), a film prepared by stroking from the melt sate (b), and a melt quenched sample after isothermal crystallization at 9 °C (c). Inset shows the splitting of the broad and strong equatorial reflection at 4.38−3.78 Å.

4.38 and 3.78 Å which can also be observed in the electron diffraction patterns. These spacings are usually measured in the fiber patterns of nylons and are

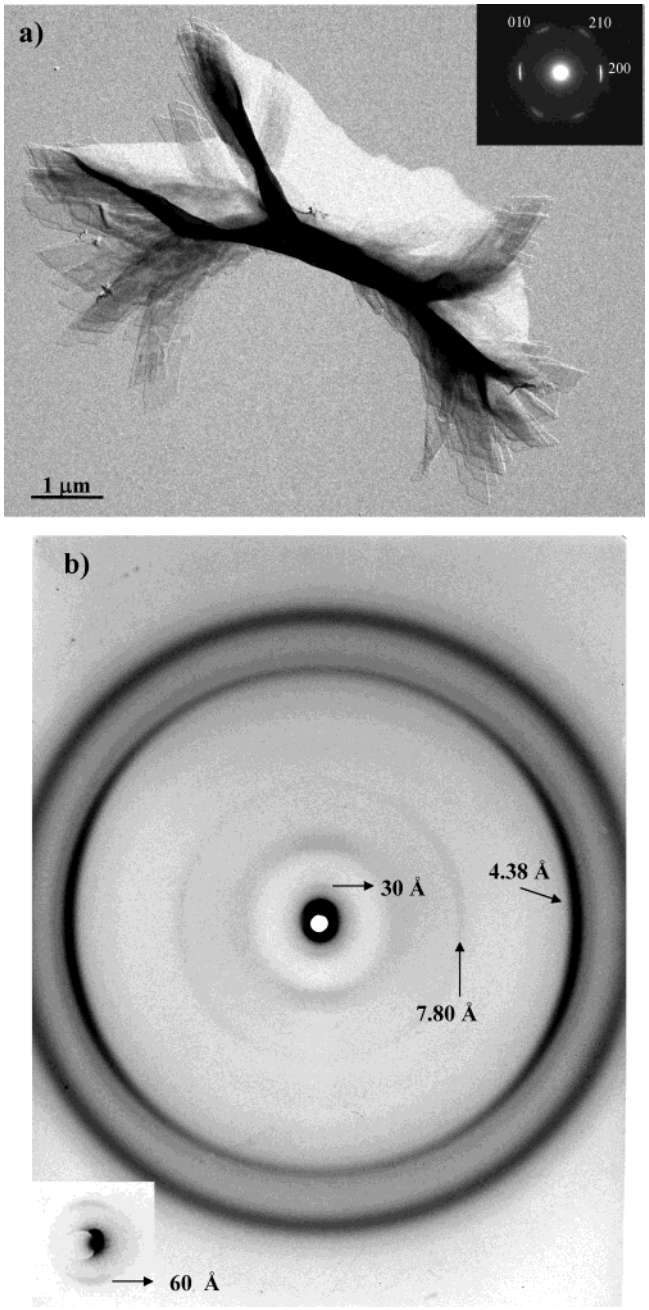

Figure 12. (a) Lamellar crystals of *i*-PEAG6 obtained by isothermal crystallization in 1,4-butanediol at 60 °C. The *hk*0 electron diffraction pattern with labeling of main reflections for a progressive sheet stacking is shown in the inset. (b) X-ray diffraction pattern of a sedimented crystals mat obtained by isothermal crystallization in 1,4-butanediol at 60 °C. Inset shows the first lamellar order observed at 60 Å in the low-angle diffraction patterns.

indicative of an oblique chain axis projected unit cell. An angle of 66° can be deduced when a 4.79 Å distance between hydrogen-bonded chains is assumed.

X-ray diffraction patterns of cold-crystallized samples (Figure 11c) indicate a new crystalline structure that may be related to the pseudohexagonal γ form of polyamides or a more disordered structure with a random orientation of amide groups that allows to establish hydrogen bonds according to a pseudohexagonal arrangement. In this way, the most intense reflection appears at 4.04 Å, and a large shortening of the chain repeat can be deduced from the (002) inner reflection at 13.4 Å.

Isothermal crystallizations were successfully undertaken in dilute 1,4-butanediol solutions at 60 °C. Thus, long sheaves with lath-shaped extremities could be attained (Figure 12a). The observed high aspect ratio can be well explained assuming that hydrogen bonds are established along the preferential grown direction, a fact that is supported by the correlation between bright field micrographs and electron diffraction patterns. Thus, the 3.78 Å reflection appears perpendicularly oriented to the long crystal axis. The (100) and (010) crystal grown faces form and angle close to 65°, which is in agreement with the reported unit cell dimensions, as well as the angle close to 50° measured between the 010 and 210 reflections.

X-ray diffraction patterns of sedimented crystals mats (Figure 12b) show the aforementioned intense reflections at 4.38 and 3.78 Å. Meridional reflections associated with lamellar orders could also be detected, indicating a regular lamellar thickness close to 60 Å. These spots make difficult the observation of 00*l* reflections and consequently the distinction between the indicated progressive and recuperative sheet stackings. However, some features points out that the single crystals adopt the former structure: (a) The 3.78 Å reflection appears disoriented in the mat patterns, despite the equatorial orientation observed for the 4.38 Å reflection. This observation can be justified taking into account the values of 90° and 58° for the β and α crystallographic angles, respectively. (b) The electron diffraction patterns show a low intensity for the 3.78 Å reflections, which in addition appear broad and diffuse. This fact is in agreement with a tilting of molecular chains with respect to the crystal basal plane, as expected for a structure with $\alpha \neq 90°$. (c) The equatorial reflection at 7.80 Å (detected in the X-ray diffraction pattern) can only be indexed as the 101 reflection (7.75 Å) of the triclinic unit cell.

The structural results obtained with *i*-PEAG6 reflect the structural complexity of poly(ester amide)s, since previous studies on compounds derived from diols, dicarboxylic acids, and amino acids suggest a different stacking[3,7] that gives rise to rectangular chain axis projected unit cells.

Conclusions

The results achieved in this investigation can be summarized as follows:

(a) Poly(ester amide)s derived from 6-amino-1-hexanol and glutaric acid with a high molecular weight can be obtained by solution polycondensation through the ester active method. Polymers show excellent film- and fiber-forming properties. On the contrary, molecular weights are limited when the synthesis involves a thermal polycondensation due to the imide ring formation.

(b) The poly(ester amide) can be processed from the melt state, since no evidence of decomposition can be detected at temperatures lower than 200 °C. Over that, imide ring formation becomes a significant degradation mechanism.

(c) Thermal behavior is characterized by a double melting peak that is associated with a recrystallization process during heating of different populations of lamellar crystals.

(d) The polymer is hydrolytically degradable through the cleavage of ester bonds. The degradation process is not accelerated by an imide ring formation, as it happens with some succinic derivatives.

(e) Degradation is enhanced by using proteolytic enzymes, such as proteinase K. On the contrary, estearases like lipase from *Pseudomona Cepacia* are less effective.

(f) i-PEAG6 crystallizes from the melt or by evaporation of concentrated formic acid solutions as negative birefringent spherulites. Kinetic crystallization studies agree with an heterogeneous nucleation and an spherulitic grown.

(g) Structural studies indicate that *i*-PEAG6 preferentially adopts an hydrogen-bonded sheet structure with an antiparallel molecular chain arrangement. Consecutive sheets are sheared along both the hydrogen-bonding and the chain axis directions. Progressive and recuperative stackings similar to those reported for the α- and *β*-forms of nylons can be found.

Acknowledgment. This research was supported by a research grant from Comisión Interministerial de Ciencia y Tecnología (CICYT) (MAT2000-0995). We are grateful to Ms. Esperanza Requena for her contribution in the synthesis and characterization of *i*-PEAG6 and also to Cristina Mallafré for her help in the manuscript preparation.

References and Notes

(1) Paredes, N.; Rodríguez-Galán, A.; Puiggalí, J. *J. Polym. Sci., Polym. Chem. Ed.* **1998**, *36*, 1271.
(2) Paredes, N.; Rodríguez-Galán, A.; Puiggalí, J.; Peraire, C. *J. Appl. Polym. Sci.* **1998**, *69*, 1537.
(3) Paredes, N.; Casas, M. T.; Puiggalí, J.; Lotz, B. *J. Polym. Sci., Polym. Phys. Ed.* **1999**, *37*, 2521.
(4) Rodríguez-Galán, A.; Pelfort, M.; Aceituno, J. E.; Puiggalí, J. *J. Appl. Polym. Sci.* **1999**, *74*, 2312.
(5) Rodríguez-Galán; Fuentes, A. L.; Puiggalí, J. *Polymer* **2000**, *41*, 5967.
(6) Rodríguez-Galán, A.; Paredes, N.; Puiggalí, J. *Curr. Trends Polym. Sci.* **2000**, *5*, 41.
(7) Paredes, N.; Casas, M. T.; Puiggalí, J. *J. Polym. Sci., Polym. Phys. Ed.* **2001**, *10*, 1036.
(8) Armelin, E.; Paracuellos, N.; Rodríguez-Galán, A.; Puiggalí, J. *Polymer* **2001**, *42*, 7923.
(9) Asin, L.; Armelin, E.; Montané, J.; Rodríguez-Galán; A.; Puiggalí, J. *J. Polym. Sci., Polym. Chem. Ed.* **2001**, *39*, 4283.
(10) Montané, J.; Armelin, E.; Asín, L.; Rodríguez-Galán, A.; Puiggalí, J. *J. Appl. Polym. Sci.* **2002**, *85*, 1815.
(11) Grigat, E.; Koch, R.; Timerman, R. *Polym. Degrad. Stab.* **1998**, *59*, 223.
(12) Botines, E.; Rodríguez-Galán, A.; Puiggalí, J. *Polymer* **2002**, *43*, 6073.
(13) Sasaki, S.; Miyauchi, M. *J. Agric. Chem. Soc. Jpn.* **1942**, *18*, 54.
(14) Kropa, E. L. U.S. 2,440,516, April 1948.
(15) Chelnokova, G. N.; Koshak, V. V. *Sb. Statei Obsch. Khim.* **1953**, *2*, 1070, 1075, 1278.
(16) Reppe, W.; Kutepow, N. V.; Wilhelm, H.; Dachs, K. (to BASF) Ger. 1,050,053, Feb 1959.
(17) Kodak Soc. Belg. 592,333, 1960.
(18) Minsk, L. M.; Abel, E. P. (to Eastman Kodak Co.) U.S. 3,316,097, April 1967.
(19) Gevaert-Agfa, Fr. 1,444,620, July 1966.
(20) Ess, R. J.; Floyd, D. E. (to General Mills, Inc.) U.S. 3,397,816, Aug 1968.
(21) Bayer, J. W. (to Owens-Illinois, Inc.) U.S. 3,749,630, July 1973.
(22) Bayer, J. W. (to Owens-Illinois, Inc.) U.S. 3,922,469, Nov 1975.
(23) Beck, A. Fr. 2,010,170, Feb 1970.
(24) Jamilkowski, D. D.; Shalaby, S. W. (to Ethicon, Inc.) U.S. 4,209,607, June 1980.
(25) Mukherjea, R. N.; Pal, S. K.; Sanyal, S. K. *J. Appl. Polym. Sci.* **1983**, *28*, 3029.
(26) Sackmann, G.; Koenig, J. H. (Bayer A. G.) Eur. Pat. Appl EP 307,778, March 1989.
(27) Xerox Corp. Nerth. Appl. 7,510,083, March 1976.
(28) Arshady, R. *Makromol. Chem.* **1984,** *185*, 2387.
(29) Gibson, H. W.; Bailey, F. C.; Mincer, J. L.; Gunther, W. H. H. *J. Polym. Sci., Polym. Chem. Ed.* **1979**, *17*, 2961.
(30) Schnar, R. L.; Weigel, P. H.; Kuhlenschmidt, M. S.; Lee, Y. C.; Roseman, S. *J. Biol. Chem.* **1978**, *253*, 7940.
(31) Langer, R.; Barrera, D. A.; Zylstra, E.; Lansbury, P. T. *J. Am. Chem. Soc.* **1993**, *115*, 11010.
(32) Sieglaff, C. L.; Hora, C. J.; Tiefenbach, J. P. (to Diamond Shamrock Corp.) U.S. 4,128,318, Dec 1978.
(33) Minoura, N.; Fujiwara, Y.; Aiba, S. (to Jpn. Kokai Tokyo Koho) JP 62,258,703, Nov 1987.
(34) Villuendas, I.; Molina, I.; Regaño, C.; Bueno, M.; Martínez de Ilarduya, A.; Galbis, J.; Muñoz-Guerra, S. *Macromolecules* **1999**, *32*, 8033.
(35) Alemán, C.; Navarro, E.; Puiggalí, J. *J. Org. Chem.* **1995**, *60*, 6135.
(36) Alemán, C.; Puiggalí, J. *J. Org. Chem.* **1997**, *62*, 3076.
(37) Navarro, E.; Alemán, C.; Puiggalí, J. *J. Am. Chem. Soc.* **1995**, *117*, 7307.
(38) Fersht, A. R.; Jenks, W. P. *J. Am. Chem. Soc.* **1970**, *92*, 5432.
(39) Van Krevelen, D. W. *Properties of Polymers*, 3rd ed.; Elsevier: Amsterdam, 1990.
(40) Avrami, M. *J. Chem. Phys.* **1940**, *8*, 212.
(41) Takayanagi, M.; Yamashita, T. *J. Polym. Sci.* **1956**, *22*, 552.
(42) Botines, E.; Franco, L.; Rodríguez-Galán, A.; Puiggalí, J. *J. Polym. Sci., Polym. Phys. Ed.* **2003**, *41*, 903.
(43) Xenopoulos, A.; Clark, E. S. In *Nylon Plastics Handbook*; Kohan, M. I., Ed.; Hanser Publishers: Munich, 1995; Chapter 5.
(44) Holmes, D. R.; Bunn, C. W.; Smith, D. J. *J. Polym. Sci.* **1955**, *17*, 159.
(45) Urpí, L.; Villaseñor, P.; Rodríguez-Galán; A.; Puiggalí, J. *J. Macromol. Chem. Phys.* **2000**, *201*, 1726.

MA0345652